fire

MDPI

Article

State-to-State Rate Constants for the $O(^3P)+H_2(v)$ System: Quasiclassical Trajectory Calculations

Alexey V. Pelevkin *, Ilya V. Arsentiev, Ilya N. Kadochnikov, Ivan A. Zubrilin, Evgeny P. Filinov and Denis V. Yakushkin

Institute of Engine and Power Plant Engineering, Samara National Research University, 34, Moskovskoye Shosse, Samara 443086, Russia; kadochnikov@phystech.edu (I.N.K.); zubrilin.ia@ssau.ru (I.A.Z.); filinov@ssau.ru (E.P.F.); yakushkin.dv@ssau.ru (D.V.Y.)

* Correspondence: pelevkin@phystech.edu

Abstract: The rate constants of elementary processes in the atom–diatom system $O(^3P) + H_2(v)$, including the processes of vibrational relaxation and dissociation, were studied using the quasiclassical trajectory method. All calculations were carried out along the ground potential energy surface (PES) $^3A''$ that was approximated by a neural network. Approximation data were obtained using *ab initio* quantum chemistry methods at the extended multi-configuration quasi-degenerate second-order perturbation theory XMCQDPT2 in a basis set limit. The calculated cross-sections of the reaction channels are in good agreement with the literature data. A complete set of state-to-state rate constants was obtained for the metathesis reaction, the dissociation and relaxation of the H_2 molecule upon collision with an O atom. According to these data, Arrhenius approximations over a wide temperature range were obtained for the thermal rate constants of considered processes. Data obtained on the dissociation constants and VT relaxation of vibrationally excited H_2 molecules can be used in constructing kinetic models describing the oxidation of hydrogen at high temperatures or highly nonequilibrium conditions.

Keywords: quasiclassical trajectory (QCT) method; state-resolved rate constants; hydrogen; atom-molecule collisions; dissociation; vibrational energy relaxation

check for updates

Citation: Pelevkin, A.V.; Arsentiev, I.V.; Kadochnikov, I.N.; Zubrilin, I.A.; Filinov, E.P.; Yakushkin, D.V. State-to-State Rate Constants for the $O(^3P)+H_2(v)$ System: Quasiclassical Trajectory Calculations. *Fire* **2024**, *7*, 220. https://doi.org/10.3390/fire7070220

Academic Editors: Jinlong Zhao, Alexey D. Kiverin and Pavel N. Krivosheyev

Received: 21 March 2024
Revised: 20 June 2024
Accepted: 25 June 2024
Published: 28 June 2024

Copyright: © 2024 by the authors. Licensee MDPI, Basel, Switzerland. This article is an open access article distributed under the terms and conditions of the Creative Commons Attribution (CC BY) license (https://creativecommons.org/licenses/by/4.0/).

1. Introduction

Modelling of combustion processes in the hydrogen–oxygen system is of great practical importance, since hydrogen is a promising fuel that allows us to improve both the efficiency and environmental characteristics of gas turbine engines and power plants [1,2]. For hydrogen as a fuel, there are a large number of kinetic mechanisms of various degrees of detail [3,4], but the problem of quantitative description of the hydrogen–oxygen kinetics cannot be considered fully solved, since there is no complete agreement between theoretical modelling and experiments [2,3]. In recent years, there was an active discussion in the literature about the necessity of taking into account the processes of vibrational relaxation in kinetic mechanisms to describe combustion and detonation [5–8], and the question of the role of vibrational excitation of radicals (for example, the HO_2 molecule) formed in chain reactions of oxidation was raised [3,9]. Moreover, there are still uncertainties in third body efficiencies for collision-induced dissociation, recombination, and molecular internal energy relaxation processes [10,11]. This work is devoted to the application of molecular dynamics methods to obtain new information about the probabilities of elementary physicochemical processes of hydrogen oxidation, which are important from both theoretical and practical points of view, for example, to improve the efficiency of modelling hydrogen combustion in future gas turbine engines.

Numerical modeling of molecular dynamics is an actively developing field of science, which has become the de facto main method to obtain new information about the rate

constants of physicochemical processes [12,13]. The progress of molecular dynamics methods is due to the availability of powerful computers, the development of computational algorithms (in particular, the increasingly widespread use of neural networks), the ability to perform numerical simulation from first principles, and the absence in a numerical experiment of some natural limitations inherent in laboratory diagnostic methods [14]. In particular, the methods of molecular dynamics allow us to obtain the most complete description of the dependence of the probabilities of physicochemical processes on the quantum states (rotational, vibrational, electronic) of reacting particles in a wide temperature range [15]. The complete sets of state-to-state rate constants acquired in this way can be used to obtain averaged characteristics of the reacting system (for example, thermal rate constants), or used to assemble kinetic models for thermally nonequilibrium gas. Such nonequilibrium models considering vibration–chemistry coupling (state-to-state [7,16–19] and multitemperature [5,6,16,20–22] models) are widely used to simulate flows with shock waves [16,17,20,21,23–28] and detonation waves [5–9], flows in a supersonic nozzle [18,29,30], gas under discharge conditions [31–33], during emission/absorption of intense radiation [34,35], in the upper layers of the Earth's atmosphere [36], to describe chemistry of the interstellar space [37,38]. Thus, the development of the methods for state-specific rate constant calculations and the generation of new data on rate constants is an important and urgent task, to which this study is devoted.

The main difficulty in estimating the state-to-state rate constants of the reactions and the energy exchange processes is that it is impossible to apply simple estimation approaches (the model of solid spheres, the capture model, the theory of the transition state, etc.) without additional assumptions and empirical corrections. To obtain state-to-state rate constants, it is necessary to use dynamic calculation methods based either on solving the equations of classical mechanics (for example, the method of quasi-classical trajectories (QCTs) [39]), or on solving the quantum dynamics equations of the system under study (for example, the real wave packets method [40]). The latter group of methods is quite difficult to implement even for simple atom–diatom systems; therefore, the main method for estimating the state-to-state rate constants used in most studies is the QCT method [21,41–52]. According to this, it should be noted that the QCT method, as any other classical method, does not take into account quantum effects, for instance, the tunneling effect and over-barrier reflection. In this paper, the implementation and application of the QCT method will be considered.

The implementation of the QCT method requires either a preliminary assignment of the entire potential energy surface (PES) of a system of colliding particles in some analytical form (PES can be obtained from ab initio calculations or based on the modelling multidimensional potentials, for example, LEPS potential [53]), or determination of the PES along each calculated trajectory "on the fly" based on calculating the energy gradient at the trajectory point (usually by ab initio methods) [54]. In this paper, the first approach was used, i.e., the PES approximation based on data from ab initio calculations and subsequent construction of the trajectory ensembles of interest, since the number of trajectories per ensemble should be large enough that the relative statistical error of the rate constant estimations is less than 10%.

A separate task is to represent the PES as a multidimensional function of the atomic nuclei coordinates, for which approximations based on the least squares method are often used, defining the PES function as a series of degrees of atomic coordinates [55]. An alternative approach is to use a neural network as a universal approximator. One such method is approximation by a neural network that accepts symmetrized coordinates as an input (PIP-NN—permutation invariant polynomials–neural network method) [50,56–58]. The use of such symmetrized coordinates makes it possible, with the existing indistinguishability in permutations of identical atoms in the reacting system, to reduce the number of PES points necessary for the approximation.

The purpose of the present work is, first, to implement the QCT method for calculating the state-to-state rate constants in the atom–diatom A + BC test system using the PIP-NN

method to approximate the PES of the system, and, second, to obtain a complete set of state-resolved rate constants for the exchange reaction A + BC→AB + C, dissociation, and VT (vibrational–translational) relaxation of BC molecules on A atoms. The $O(^3P) + H_2$ system was chosen as such a test system, since it was previously studied in detail by molecular dynamics methods in the works of other authors [37,59–61], which will allow us to validate our implementation of the QCT method. Nevertheless, in previous studies [37,59–61], the probabilities of dissociation and VT relaxation of $H_2(v)$ molecules on the O atom were not considered. So, the QCT method for these processes, as far as the authors know, is used for the first time.

2. Methodology

2.1. PES Approximation

All calculations of the PES of the $O(^3P) + H_2$ system along the ground state $^3A''$ surface were carried out at the level of the extended multi-configuration quasi-degenerate second-order perturbation theory XMCQDPT2 [62]. We choose this method because XMCQDPT2 combines an acceptable calculation cost and sufficient accuracy in calculating the dynamic correlation energy for similar molecular systems [63–66]. As an initial approximation of the wave function, the results of the calculation by the multi-configuration self-consistent field method with a dynamic choice of weights DW-CASSCF [67] was used. Such a choice of a multi-configuration calculation method is associated with the need for a smooth construction of the PES, which is most likely provided by the DW-CASSCF method (see ref. [68] for details). The size of the active space specified in the DW-CASSCF method is 8 electrons distributed in 6 orbitals, i.e., the full valence space for the considered system. The main set of basis functions in all calculations is the family of Dunning basis sets with diffuse functions aug-cc-pVXZ (X = D, T, Q) [69]. Based on calculations in the basis sets aug-cc-pVXZ (X = D, T, Q), the energies were calculated at each point of the PES in the limit basic set aug-cc-pV∞Z; for MCSCF energies, the exponential extrapolation scheme [70,71], and for XMCQDPT2 energies, the scheme using Riemann zeta function [72], were utilized. All *ab initio* calculations were carried out in the Firefly QC v.8.2.0 software package [73], partially based on the GAMESS (US) [74] source code.

The obtained set of PES data was approximated using the PIP-NN method [56]. This approach to fit PES has important advantages: the universality of the method, the availability of neural network training tools (for example, TensorFlow [75], PyTorch [76], Keras [77] software packages, etc.), the ability to implement the analytical nuclear gradient at any point of the PES. At the same time, the main drawback of this approach is related to the peculiarity of the neural network device that slows down calculations comparing with, for example, LEPS potential; for a neural network with a sigmoid activation function or a hyperbolic tangent, the main calculation time of the output neuron is spent on multiple calculations of this function, as well as matrix–vector multiplication operations.

In the framework of the PIP-NN method, before constructing and training a neural network that plays the role of a universal approximator, it is necessary to transform the Cartesian coordinates of atomic nuclei into symmetrized coordinates. Since the $O(^3P) + H_2$ system corresponds to the AB_2 type, the general form of symmetrized coordinates is already known via Morse coordinates [78]:

$$\begin{cases} G_1 = \exp\left(-\lambda r_{H_1H_2}\right) \\ G_2 = \exp\left(-\lambda r_{OH_1}\right) + \exp\left(-\lambda r_{OH_2}\right) \\ G_3 = \exp\left(-\lambda r_{OH_1}\right) \cdot \exp\left(-\lambda r_{OH_2}\right) \end{cases} \quad (1)$$

Here, r_{XY} is the distance between X and Y atoms in Å, and λ is a dimensional coefficient equal to 1–2 Å^{-1}. In general, it is necessary to solve a combinatorial problem with respect to permutations of atoms and the corresponding permutations of interatomic distances. Software packages such as MAGMA [79] and SINGULAR [80], which are able to determine permutation groups based on a given permutation matrix, help in solving these problems.

The coordinates obtained in this way within the PIP-NN approach are fed to the input of the neural network, and at the output, the neural network gives the potential energy value.

2.2. Rate Constant Estimation

The direct calculation of the rate constants by the QCT method is based on a statistical analysis of the outcomes of trajectory ensembles with specified conditions. We will briefly describe the stages of all calculations that eventually lead to estimates of the rate constants of interest, according to the methodology from [39,81,82].

First of all, it is necessary to convert the Cartesian coordinates of the atomic nuclei into Jacobi coordinates for the atom–diatomic molecule system. In the case of the $O(^3P) + H_2$ system, these are the three coordinates of the H_1 atom relative to the H_2 atom, the three coordinates of the $O(^3P)$ atom relative to the mass center of the H_1 H_2 molecule, and the three coordinates of the mass center of the entire $O(^3P)H_1H_2$ system. After the corresponding linear transformation, the Hamiltonian of the system will take the form:

$$H(\mathbf{p},\mathbf{q}) = \sum_{i=1}^{3} \frac{p_i^2}{2\mu_{H_1H_2}} + \sum_{i=4}^{6} \frac{p_i^2}{2\mu_{O,H_1H_2}} + \sum_{i=7}^{9} \frac{p_i^2}{2M_{OH_1H_2}} + V(\mathbf{q}). \quad (2)$$

Here, μ represents appropriate reduced masses, $M_{OH_1H_2}$ is the total mass of the entire system, $\mathbf{q}$ or q_i is the Jacobi coordinates, $\mathbf{p}$ or p_i is the generalized momentum corresponding to $\mathbf{q}$, and $V(\mathbf{q})$ is the potential energy of the system at the point with the coordinates $\mathbf{q}$. The resulting Hamiltonian (2) allows us to compose the equations of motion of Hamiltonian mechanics, which were then solved numerically using an explicit one-step Runge–Kutta–Merson method of the 4th order of accuracy with a variable integration step starting from 0.02 fs.

Each ensemble of trajectories was set by initial conditions which are described in detail in [39,81,82]. Here, we only note following. The calculation of the reaction cross-section was carried out without scanning over the impact parameter; each ensemble of trajectories was set only by the vibrational and rotational numbers of the H_2 molecule and the kinetic energy of the incoming $O(^3P)$ atom. Starting and final distances between colliding particle are 8 Å; the upper limit of collision energy is 9 eV. Also, we note that rotational quantum number J is estimated in the same way as described in [82] and vibrational quantum number v is chosen as the nearest number corresponding to the precalculated rovibratinal energy level of a product molecule (in this sytem, the OH or H_2 molecules).

Also, to construct the initial conditions and to analyze each trajectory, it is necessary to know the rovibrational levels of H_2 and OH molecules, but the approximation of the anharmonic Morse potential may be inaccurate when describing upper rovibrational levels. Therefore, the energy levels of diatomic molecules were determined by numerically solving the radial component of the stationary Schrödinger equation for a diatomic molecule with the LEVEL16 program [83]. However, it is worth noting that this program, alongside bound states, also calculates the energy levels of quasi-bound states [83]. Despite the fact that some of the quasi-bound states may be metastable and have a lifetime of tens of hours, such states will not be considered within the framework of the QCT method, and the trajectories that led to such an outcome will be attributed to the dissociation process.

According to the methodology described above, it becomes possible to calculate the cross-sections of the following reactions in this system:

$$\begin{gathered} O(^3P) + H_2(v_1, J_1) \rightarrow H + OH(v_2, J_2), \\ O(^3P) + H_2(v_1, J_1) \rightarrow O(^3P) + H_2(v_2, J_2), \\ O(^3P) + H_2(v, J) \rightarrow O(^3P) + H + H. \end{gathered} \quad (3)$$

The reaction cross-section was calculated using the ratio of the trajectory number N_R that led to the required outcome to the total number of trajectories of the ensemble N according to the formula from [39,48,50,51,81,82]:

$$\sigma(v, J, E) \approx \pi b_{\max}^2 \frac{N_R}{N} \tag{4}$$

with the statistical error

$$\Delta(v, J, E) \approx \pi b_{\max}^2 \frac{N_R}{N} \sqrt{\frac{N - N_R}{N N_R}}. \tag{5}$$

Here, $b_{\max}$ is the maximum value of the impact parameter at which the probability of a particular process (reaction, dissociation, or VT relaxation process) is above zero, and E is the kinetic energy of the incoming $O(^3P)$ atom. In all calculations, the total number of trajectories that compose one ensemble was equal to 30,000, and the highest kinetic energy of the $O(^3P)$ atom was equal to 9 eV.

On the basis of the obtained cross-sections, the rate constants $k(v, J, T)$ and their error $\Delta k(v, J, T)$ were calculated by the following formulas:

$$\begin{aligned} k(v, J, T) &= N_A \frac{g_{PES}^e}{g_R^e} \sqrt{\frac{8 k_B T}{\pi \mu_{A,BC}}} \int_0^\infty \sigma(v, J, E) \exp\left(-\frac{E}{k_B T}\right) \frac{dE}{(k_B T)^2}, \\ \Delta k(v, J, T) &= N_A \frac{g_{PES}^e}{g_R^e} \sqrt{\frac{8 k_B T}{\pi \mu_{A,BC}}} \int_0^\infty \Delta(v, J, E) \exp\left(-\frac{E}{k_B T}\right) \frac{dE}{(k_B T)^2}. \end{aligned} \tag{6}$$

Here, g_{PES}^e and g_R^e are the electronic statistical weights of the studied PES and reagents, respectively, and k_B is the Boltzmann constant. The integrals of Formula (6) were calculated numerically with piecewise linear interpolation of the reaction cross-section $\sigma(v, J, E)$:

$$\sigma(v, J, E) = a_i E + b_i, \tag{7}$$

where $a_i = \dfrac{\sigma_i - \sigma_{i-1}}{E_i - E_{i-1}}$ and $b_i = \dfrac{\sigma_{i-1} E_i - \sigma_i E_{i-1}}{E_i - E_{i-1}}$. Such an approximation of the reaction cross-section makes it possible to calculate the rate constant $k(T)$ by simple summation according to the following formula (the error of such a numerical approach is many times smaller than the statistical error of trajectory calculations [81]):

$$\begin{aligned} k(v, J, T) = N_A \frac{g_{PES}^e}{g_R^e} \sqrt{\frac{8 k_B T}{\pi \mu_{A,BC}}} \int_0^\infty \sigma(v, J, E) \exp\left(-\frac{E}{k_B T}\right) \frac{dE}{(k_B T)^2} \approx \\ N_A \frac{g_{PES}^e}{g_R^e} \sqrt{\frac{8}{\pi \mu_{A,BC} k_B T}} \times \\ \times \sum_{i=0}^{n} \left[\exp\left(-\frac{E}{k_B T}\right) \left(a_i \left(E^2 + 2 E k_B T + 2 (k_B T)^2 \right) + + b_i (E + k_B T) \right) \right] \Bigg|_{E_{i-1}}^{E_i}. \end{aligned} \tag{8}$$

From the obtained vibrational–rotational state-to-state rate constants (6), it is possible to determine the vibrational state-resolved rate constants $k_v(T)$ (assuming that the translational and rotational degrees of freedom of the reagents and the products are in equilibrium) and the thermal equilibrium rate constant $k_{therm}(T)$ as follows:

$$k_v(T) = \sum_{J=0}^{M(v)} w(v, J, T) k(v, J, T), \tag{9}$$

$$k_{therm}(T) = \sum_{v=0}^{N} \sum_{J=0}^{M(v)} w(v, J, T) k(v, J, T), \tag{10}$$

where $w(v, J, T)$ is the normalized population of the H_2 energy level with the vibrational and rotational numbers v and J, N is the number of vibrational levels of the molecule H_2, and $M(J)$ is number of rotational levels in the v-th vibrational level.

3. Results and Discussion

For the construction of the full PES of the $O(^3P) + H_2$ system along the ground state $^3A''$ surface, 6650 energies for the training set and 1089 energies for the test set were calculated according to the methodology of this work. Several neural networks of the multilayer perceptron type with two hidden layers were trained. The neural network with 45 neurons in the first hidden layer and 55 in the second was chosen because it gives the smallest RMS error of about 10 meV after training. In Figure 1 the minimum energy path for reaction $O(^3P)+H_2 \rightarrow H+O_2$ on the approximated PES is depicted. It is important to note that the result obtained within the framework of the transition state theory energy barrier of the exchange reaction turned out to be lower ($E_a = 11.5$ kcal/mole with zero point energy (ZPE) and $E_a \approx 11$ kcal/mole without ZPE) than the corresponding values from [84] ($E_a = 13$ kcal/mole) or from [85] ($E_a = 13.6$ kcal/mole). This difference is caused by a different level of theory in *ab initio* calculations. In [59], the PES was used from [84], where the mainframe level of theory was the ICCI method, whereas in this work, XMCQDPT2 was used. In Table 1, distances between atoms in critical points (linear orientation) on the target PES are presented along with corresponding values from [85]. It could be seen that these geometry properties of critical points are in good agreement with the results of [85].

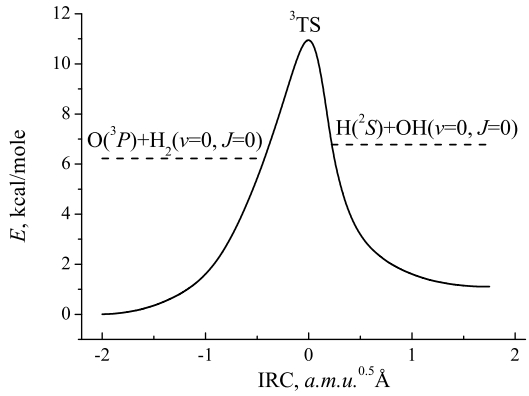


Figure 1. The minimum energy path for reaction $O(^3P)+H_2 \rightarrow H+O_2$ obtained on approximated PES by PIP-NN method.

Table 1. Geometry properties of critical points (linear orientation) obtained in this work on the $^3A''$ PES of the $O(^3P) + H_2$ system.

Structure	r_{OH}, Å	r_{HH}, Å
O−HH	2.828 (2.996) [1]	0.741 (0.729) [1]
OH−H	0.970 (0.953) [1]	2.691 (4.079) [1]
^{3}TS	1.239 (1.193) [1]	0.882 (0.872) [1]

[1] Values in brackets are taken from [85].

To validate the robustness of the methodology described above for obtaining state-to-state rate constants and assess the overall correctness of its specific implementation, it is fruitful to compare predictions of our work with the results of QCT and direct quantum dynamic calculations performed by other authors. For the considered system $O(^3P) + H_2$, the data on the cross-sections and state-specific rate constants for the processes $O(^3P) + H_2(v, J) \rightarrow H + OH$ are widely presented in the literature. So, in Figure 2, the cross-sections for the $O(^3P) + H_2(v, J = 0) \rightarrow H + OH$ reaction from our QCT estimates are presented in comparison with the similar QCT results from [59]. One can notice a

slight overestimation of cross-sections in our modelling compared to [59]. This discrepancy may be the reflection of the properties of the two PES used in different works to perform trajectory calculations, and (as was mentioned above) the most significant difference in the PES properties could be the lower energy barrier of the exchange reaction in the frame of our simulations when compared to that in [59].

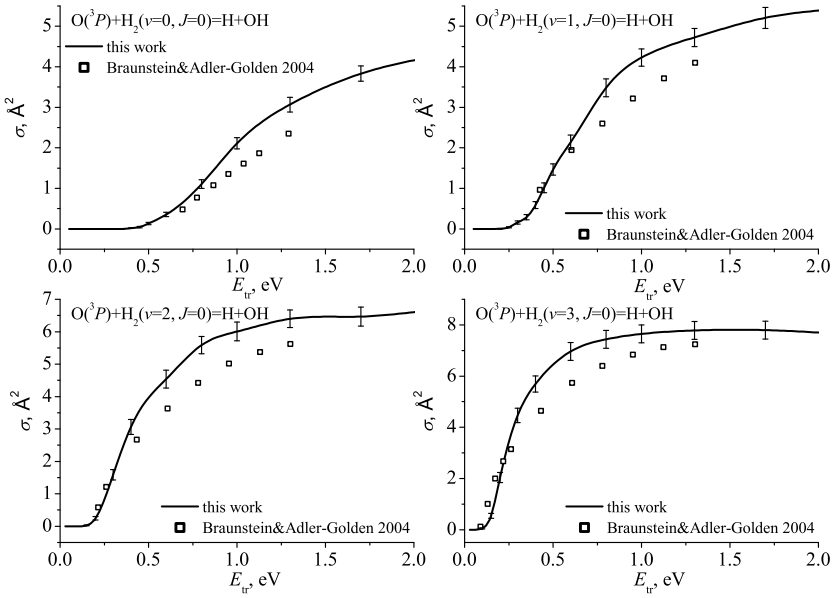


Figure 2. The $O(^3P) + H_2(v = 0...3, J = 0) \rightarrow H + OH$ reaction cross-section along the lower $^3A''$ PES, calculated according to our methodology (solid lines with error bars) and using the QCT method from [59] (markers from Braunstein and Adler-Golden 2004).

Figure 3 shows a comparison of the state-to-state rate constants found by the QCT method in this work and obtained on the basis of quantum dynamics calculations in [37]. This comparison shows a good qualitative agreement of the results of the two computational studies. Nevertheless, for reaction channels with a quantum number $v > 4$ and the difference in the values of the rate constants determined by different methods can be significant, and for the temperatures $T < 500$ K, they can reach an order of magnitude.

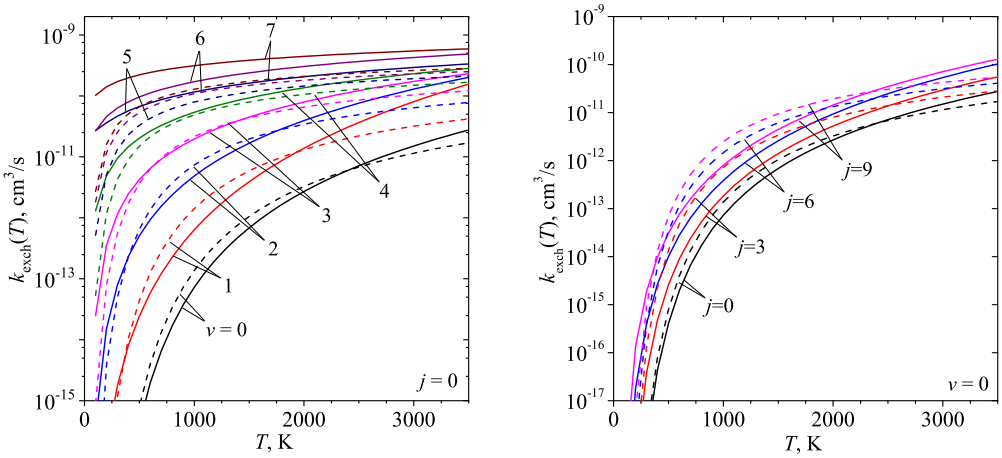


Figure 3. Comparison of the $O(^3P) + H_2(v, j) \rightarrow H + OH$ state-to-state reaction rate calculated in this work by the QCT method (dashed lines) and obtained in [37] using quantum dynamics calculations (solid lines).

A comparison of the thermal equilibrium $O(^3P) + H_2 \rightarrow H + OH$ reaction rate constant, calculated in this work via the QCT method and obtained in [37] on the basis of

quantum dynamics calculations, is shown in Figure 4. In addition, Figure 4 shows an estimate of this rate constant obtained using the non-variational transition state theory adjusted for the tunnel effect and various Arrhenius approximations of the rate constant used in the kinetic models [86–88]. One can notice an expected overestimation of the rate constant by the transition state theory, while the QCT method gives closer values, although somewhat higher at $T < 2500$ K, relative to the known data. Such an overestimation has the same cause as in the case of the reaction cross-section—lowering the energy barrier at the XMCQDPT2/aug-cc-pV∞Z level of theory. The discrepancy in the values of the rate constant at $T > 2500$ K is explained by the different temperature ranges for which the Arrhenius approximation was obtained. Note that our estimation for the thermal equilibrium rate constant under consideration can be approximated with good accuracy in the temperature range $T = 100 - 5000$ K by the following Arrhenius dependence ($cm^3/(mole \cdot s)$):

$$k^0_{exch}(T) = 1.21 \cdot 10^9 T^{1.37} \exp(-3684/T). \quad (11)$$

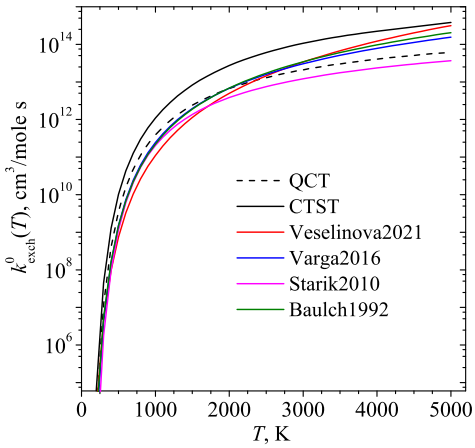


Figure 4. Thermal rate constant of the reaction O+H_2 → H+OH along the lower $^3A''$ PES, obtained by the QCT method (QCT), the non-variational transition state theory (CTST), quantum dynamics calculations (Veselinova2021 [37]), as well as used in known kinetic mechanisms (Varga2016 [86], Starik2010 [87], Baulch1992 [88]).

For the dissociation reaction and the VT relaxation process of H_2 molecules in collision with O atoms, there are no data on rate constants in the literature (as far as the authors know). Nevertheless, it is interesting to compare the estimates of the rate constants of these processes obtained by the QCT method with the available information on the rates of dissociation and VT relaxation of hydrogen molecules in collisions with other partners. For the dissociation process, such a comparison is presented in Figure 5. It turns out that the equilibrium rate constant of the dissociation of H_2 obtained in this work significantly exceeds those with the different partners available in the literature. However, at temperatures $T > 1000$ K, the dissociation rate constant of hydrogen upon collision with O atoms coincides by the order of magnitude with the dissociation rate constants in collision with H and H_2O. The thermal equilibrium rate constant of H_2 dissociation obtained in this work in the temperature range $T = 100 - 5000$ K can be described with good accuracy using the double Arrhenius dependence ($cm^3/(mole\ s)$):

$$k^0_{dis}(T) = 1.92 \cdot 10^9 T^{0.63} \exp(-39143/T) + 1.21 \cdot 10^{15} T^{0.19} \exp(-47567/T). \quad (12)$$

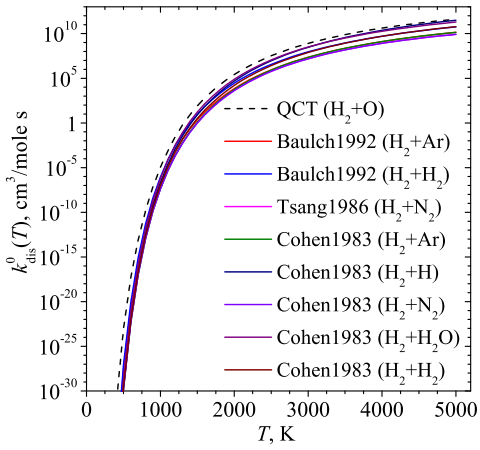


Figure 5. Comparison of the thermal H_2 + O = 2H + O dissociation rate constant calculated in this paper with hydrogen dissociation rate constants presented in other works (Baulch1992 [88], Tsang1986 [89], Cohen1983 [90]).

Figure 6 shows a comparison of the VT relaxation time of H_2 molecules in collisions with various partners. Note that for the processes of hydrogen relaxation on H, H_2, and O, the relaxation time was determined using the VT rate constant of the transition from the first excited vibrational level to the ground state:

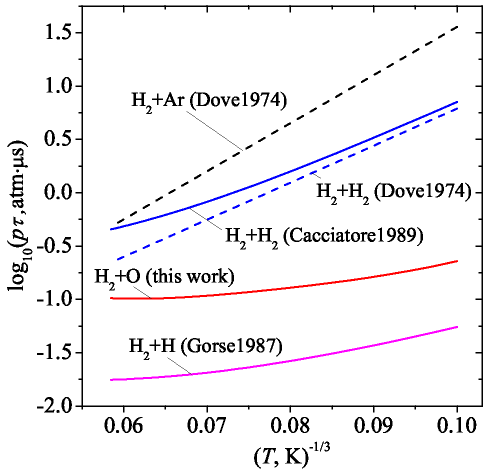


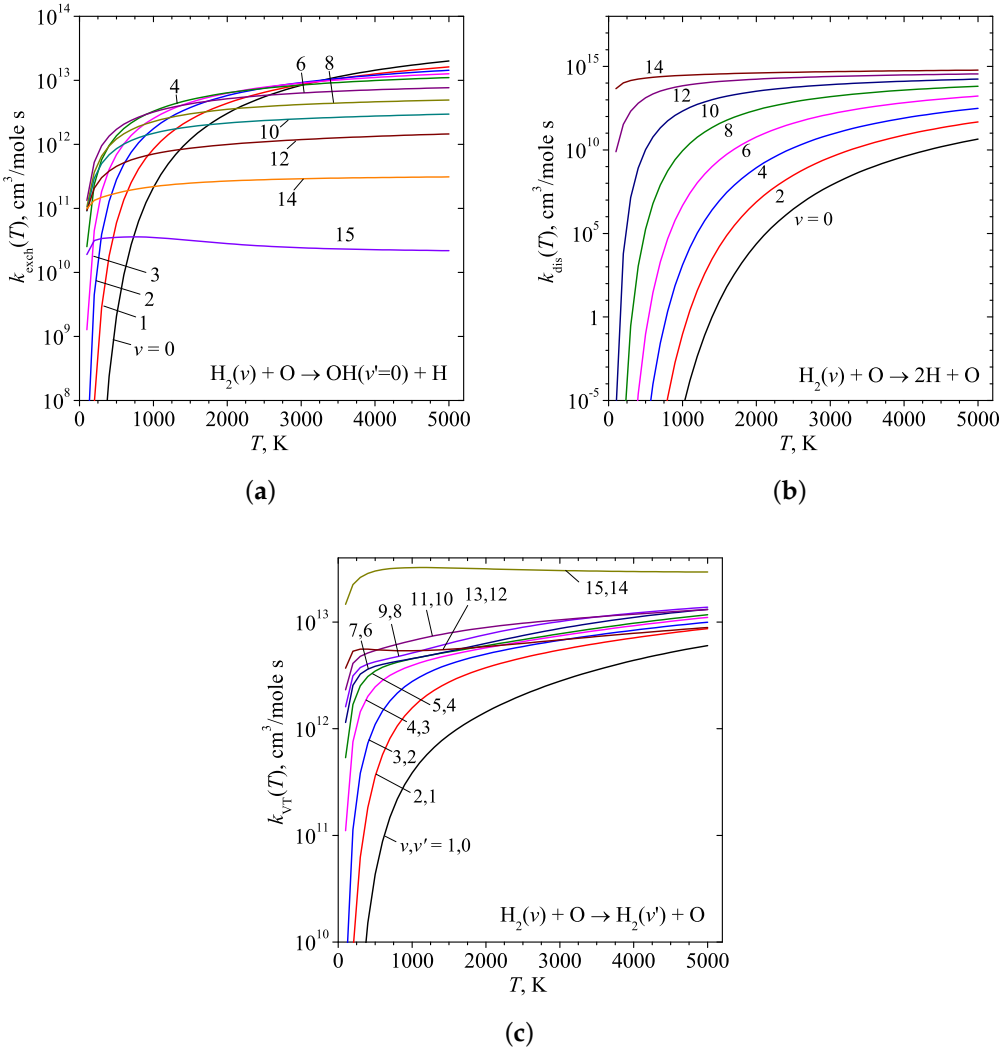
Figure 6. Vibrational relaxation time of H_2 molecules on various collisional partners. Dashed lines are experimental data (Dove1974 [91]), while solid lines are calculation results (Cacciatore1989 [92], Gorse1987 [41]).

$$p\tau = \frac{k_B T}{k_{V,T}^{1,0}(1 - \exp(-\theta_v / T))}. \quad (13)$$

Here, $k_{V,T}^{1,0}$ is the VT relaxation rate constant, and θ_v is the characteristic vibrational temperature. It can be seen from Figure 6 that according to the results of calculations performed in this work, the vibrational relaxation of H_2 proceeds faster on the O atom than on the Ar atom, but slower than on the H atoms, which is consistent with the qualitative expectations of the dependence of the relaxation time of the molecule on the mass of the collisional partner, expressed, for example, in the well-known Millikan–White formula [93]. At the same time, the results of the calculation using the QCT method predict a more effective VT relaxation of H_2 in collisions with O atoms than in collisions with molecular hydrogen. It

can be assumed that this effect is due to the fact that a molecule as a collisional partner, in addition to translational degree of freedom, has rotational and vibrational freedom, unlike a single atom.

The lack of data in the literature on the probabilities of dissociation and VT relaxation of H_2 molecules in collision with O atoms is due to the fact that the exchange reaction O+H_2 → H+OH is considered as a more probable outcome of the collision of H_2 and O and hence is more important for kinetic models. State-resolved rate constants for these processes calculated in line with Equation (9) are shown in Figure 7. The comparison shows that for H_2 molecules in the ground vibrational state, the exchange reaction is indeed a much more probable process than dissociation. However, for vibrationally excited H_2 molecules, the rate constants of dissociation and VT relaxation upon collision with O can be comparable or even many times higher than the corresponding exchange reaction constants. Thus, the data obtained in this paper on the state-to-state rate constants for dissociation and VT relaxation of molecular hydrogen can be an important addition for the kinetic models describing hydrogen oxidation at high translational temperatures or under essentially nonequilibrium conditions. Note that the convenient approximations of vibrationally resolved rate coefficients estimated in this study are available as the Supplementary Materials.



(**a**) (**b**) (**c**)

Figure 7. The state-to-state rate constants of the exchange reaction (**a**), dissociation (**b**), and VT relaxation (**c**) of H_2 molecules in collision with O atoms calculated with the QCT method.

4. Conclusions

In this study, an implementation of the QCT method was created for atom–diatom systems using the PES approximation of this reacting system by a neural network. Using this implementation, cross-sections and state-to-state rate constants for exchange reactions, dissociation, and VT relaxation processes were calculated for the $O(^3P) + H_2$ system. Based on the data on the state-to-state rate constants for exchange and dissociation reactions, Arrhenius approximations of thermal equilibrium rate constants over a wide temperature range were found.

It was shown that the cross-sections and rate constants obtained in this work for the exchange reactions $O(^3P) + H_2(v, J = 0) \rightarrow H + OH$ are in good qualitative agreement with the results of the QCT and the quantum dynamics method calculations presented in the works of other authors [37,59]. In addition, our estimation of the thermal equilibrium rate constant for the exchange reaction is in good agreement with the corresponding rate constants used in various kinetic models [86–88].

As far as the authors are aware, there are no reliable data on the rate constants of dissociation and VT relaxation of H_2 molecules in collision with O atoms in the literature, and the study of these processes in the frame of the QCT method is the novelty of this work. And for the first time, the full set of vibrationally resolved rate constants for metathesis reaction, VT relaxation, and dissociation in the system $^3A''$ $O(^3P) + H_2$ was obtained by the QCT method and tabulated in a convenient form (see Supplementary Materials). A comparative analysis of the obtained state-to-state rate constants showed that when H_2 on the lower vibrational levels ($v < 5$) collides with an O atom, the probability of its dissociation is negligible compared to the probability of an exchange reaction (however, this difference decreases with increasing temperature). But for the upper vibrational levels of the hydrogen molecule, the rate constants of dissociation and VT relaxation of H_2 on O are comparable or may even exceed the corresponding state-resolved rate constants of the exchange reaction. Thus, the rate constants of dissociation and VT relaxation of H_2 on O obtained in this work can be useful in constructing kinetic models describing hydrogen oxidation under thermal nonequilibrium conditions or at high temperatures.

The results of this work make it possible to increase the efficiency of modeling processes in gas turbine power plants using promising types of fuel, such as methane–hydrogen mixtures or pure hydrogen at high-temperature conditions inherent in hydrogen fuels.

In the future, it is planned to refine the calculation of the rate constants of energy exchange processes in this system, since, in this work, the interaction of the $O(^3P)$ atom and the H_2 molecule along the $^3A'$ and the first excited $^3A''$ terms of this system was not taken into account. In addition, due to the versatility of our PES approximation method, the created computational complex can be easily adapted for different triatomic systems and other configurations of collisions, for example, for a recombination reaction A+B+C.

Supplementary Materials: The following supporting information can be downloaded at: https://www.mdpi.com/article/10.3390/fire7070220/s1, Table S1: $H_2(v)$ + O = 2H + O; Table S2: $H_2(v)$ + O = $OH(v')$ + H; Table S3: $H_2(v)$ + O = $H_2(v')$ + O.

Author Contributions: A.V.P.: conceptualization, methodology, software, writing—review and editing. I.V.A.: data curation, writing—review and editing, visualization. I.N.K.: conceptualization, methodology, validation, visualization, original draft preparation. I.A.Z.: funding acquisition, project administration, conceptualization, supervision. E.P.F.: formal analysis, validation. D.V.Y.: writing—review and editing, visualization. All authors have read and agreed to the published version of the manuscript.

Funding: The work was supported by project FSSS-2022-0019, implemented within the framework of the federal project "Development of human capital in the interests of regions, industries and the research and development sector", and consequently, "New laboratories were created, including those under the guidance of young promising researchers".

Institutional Review Board Statement: Not applicable.

Informed Consent Statement: Informed consent was obtained from all subjects involved in the study.

Data Availability Statement: The raw data supporting the conclusions of this article will be made available by the authors on request.

Acknowledgments: The authors are grateful to their colleagues Alexander S. Sharipov and Boris I. Loukhovitski for stimulating discussions.

Conflicts of Interest: The authors declare no conflicts of interest.

Abbreviations

The following abbreviations are used in this manuscript:

QCT	quasiclassical trajectory
PES	Potential energy surface
ZPE	zero point energy
VT relaxation	vibrational–translational relaxation
PIP-NN	permutation invariant polynomials–neural network
XMCQDPT2	extended multi-configuration quasi-degenerate second-order perturbation theory
DW-CASSCF	dynamically weighted complete active space self-consistent field method

References

1. Shchepakina, E.A.; Zubrilin, I.A.; Kuznetsov, A.Y.; Tsapenkov, K.D.; Antonov, D.V.; Strizhak, P.A.; Yakushkin, D.V.; Ulitichev, A.G.; Dolinskiy, V.A.; Hernandez Morales, M. Physical and Chemical Features of Hydrogen Combustion and Their Influence on the Characteristics of Gas Turbine Combustion Chambers. *Appl. Sci.* **2023**, *13*, 3754. [CrossRef]
2. Rolo, I.; Costa, V.A.F.; Brito, F.P. Hydrogen-Based Energy Systems: Current Technology Development Status, Opportunities and Challenges. *Energies* **2024**, *17*, 180. [CrossRef]
3. Skrebkov, O.V.; Kostenko, S.S.; Smirnov, A.L. Vibrational nonequilibrium in reaction hydrogen with oxygen (review). *Zhurnal Tekhnicheskoj Fiz.* **2023**, *93*, 1073–1093. (In Russian) [CrossRef]
4. Urzay, J.; Kseib, N.; Davidson, D.F.; Iaccarino, G.; Hanson, R.K. Uncertainty-quantification analysis of the effects of residual impurities on hydrogen-oxygen ignition in shock tubes. *Combust. Flame* **2014**, *161*, 1–15. [CrossRef]
5. Voelkel, S.; Masselot, D.; Varghese, P.L.; Raman, V. Analysis of Hydrogen-Air Detonation Waves with Vibrational Nonequilibrium. *AIP Conf. Proc.* **2016**, *1786*, 070015.
6. Shi, L.; Shen, H.; Zhang, P.; Zhang, D.; Wen, C. Assessment of vibrational non-equilibrium effect on detonation cell size. *Combust. Sci. Technol.* **2017**, *189*, 841–853. [CrossRef]
7. Kadochnikov, I.N.; Arsentiev, I.V. Modelling of vibrational nonequilibrium effects on the H2–air mixture ignition under shock wave conditions in the state-to-state and mode approximations. *Shock Waves* **2020**, *30*, 491–504. [CrossRef]
8. Smirnov, V.N.; Vlasov, P.A. Effects of hydrocarbon impurities, vibrational relaxation, and boundary-layer-induced pressure rise on the ignition of H_2–O_2–Ar mixtures behind reflected shock waves. *Int. J. Hydrogen Energy* **2021**, *46*, 9580–9594. [CrossRef]
9. Skrebkov, O.V.; Kostenko, S.S.; Smirnov, A.L. Vibrational nonequilibrium and reaction heat effect in diluted hydrogen-oxygen mixtures behind reflected shock waves at 1000<T<1300 K. *Int. J. Hydrogen Energy* **2020**, *45*, 3251–3262.
10. Barbet, M.C.; Burke, M.P. Impact of "missing" third-body efficiencies on kinetic model predictions of combustion properties. *Proc. Combust. Inst.* **2021**, *38*, 425–432. [CrossRef]
11. Bertolino, A.; Frassoldati, A.; Cuoci, A.; Parente, A. Estimation of third body efficiencies from experimental data: Application to hydrogen combustion. *Int. J. Hydrogen Energy* **2023**, *48*, 24504–24520. [CrossRef]
12. Houston, P.L. *Chemical Kinetics and Reaction Dynamics*; Courier Corporation: Chelmsford, MA, USA, 2012.
13. Henriksen, N.E.; Hansen, F.Y. *Theories of Molecular Reaction Dynamics: The Microscopic Foundation of Chemical Kinetics*; Oxford University Press: Oxford, UK, 2018.
14. Herschbach, D.R. Molecular Dynamics of Elementary Chemical Reactions (Nobel Lecture). *Angew. Chem. Int. Ed. Engl.* **1987**, *26*, 1221–1243. [CrossRef]
15. Leone, S.R. State-Resolved Molecular Reaction Dynamics. *Annu. Rev. Phys. Chem.* **1984**, *35*, 109–135. [CrossRef]
16. Capitelli, M.; Armenise, I.; Gorse, C. State-to-state approach in the kinetics of air components under re-entry conditions. *J. Thermophys. Heat Transfer* **1997**, *11*, 570–578. [CrossRef]
17. Kadochnikov, I.N.; Loukhovitski, B.I.; Starik, A.M. Kinetics of plasmachemical processes in the expanding flow of nitrogen plasma. *Phys. Scr.* **2013**, *88*, 058306. [CrossRef]
18. Colonna, G.; Capitelli, M. Self-consistent model of chemical, vibrational, electron kinetics in nozzle expansion. *J. Thermophys. Heat Transf.* **2001**, *15*, 308–316. [CrossRef]
19. Campoli, L.; Kustova, E.; Maltseva, P. Assessment of Machine Learning Methods for State-to-State Approach in Nonequilibrium Flow Simulations. *Mathematics* **2022**, *10*, 928. [CrossRef]

20. Park, C. Review of chemical-kinetic problems of future NASA missions. I-Earth entries. *J. Thermophys. Heat Transf.* **1993**, *7*, 385–398. [CrossRef]
21. Zhang, W.; Wang, X.; Zhang, Z.; Su, T. Numerical Investigation on the Jet Characteristics and the Heat and Drag Reductions of Opposing Jet in Hypersonic Nonequilibrium Flows. *Aerospace* **2022**, *9*, 554. [CrossRef]
22. Kustova, E.; Mekhonoshina, M.; Bechina, A.; Lagutin, S.; Voroshilova, Y. Continuum Models for Bulk Viscosity and Relaxation in Polyatomic Gases. *Fluids* **2023**, *8*, 48. [CrossRef]
23. Treanor, C.E.; Adamovich, I.V.; Williams, M.J.; Rich, J.W. Kinetics of nitric oxide formation behind shock waves. *J. Thermophys. Heat Transf.* **1996**, *10*, 193–199. [CrossRef]
24. Kustova, E.V.; Nagnibeda, E.A.; Shevelev, Y.D.; Syzranova, N.G. Comparison of different models for non-equilibrium CO_2 flows in a shock layer near a blunt body. *Shock Waves* **2011**, *21*, 273–287. [CrossRef]
25. Surzhikov, S.; Reynier, P.; Seller, G.; Taccogna, F. Radiative aerothermodynamics of entering space vehicles: Toward the use of state-to-state approach. *Open Plasma Phys. J* **2014**, *7*, 127–154. [CrossRef]
26. Gimelshein, S.F.; Wysong, I.J.; Fangman, A.J.; Andrienko, D.A.; Kunova, O.V.; Kustova, E.V.; Morgado, F.; Garbacz, C.; Fossati, M.; Hanquist, K.M. Kinetic and continuum modeling of high-temperature air relaxation. *J. Thermophys. Heat Transf.* **2022**, *36*, 870–893. [CrossRef]
27. Aiken, T.T.; Boyd, I.D. Analysis of Critical Rate Processes for Ionization in Shock-Heated Air. In Proceedings of the AIAA AVIATION 2023 Forum, San Diego, CA, USA, 12–16 June 2023; p. 3330.
28. Zhang, P.; Gao, W.; Niu, Q.; Dong, S. Numerical Analysis of Aerodynamic Thermal Properties of Hypersonic Blunt-Nosed Body with Angles of Fire. *Energies* **2023**, *16*, 1740. [CrossRef]
29. Guy, A.; Bourdon, A.; Perrin, M.Y. Consistent multi-internal-temperatures models for nonequilibrium nozzle flows. *Chem. Phys.* **2013**, *420*, 15–24. [CrossRef]
30. Zidane, A.; Haoui, R.; Sellam, M.; Bouyahiaoui, Z. Numerical study of a nonequilibrium H_2-O_2 rocket nozzle flow. *Int. J. Hydrogen Energy* **2019**, *44*, 4361–4373. [CrossRef]
31. Starikovskiy, A.; Aleksandrov, N. Plasma-assisted ignition and combustion. *Prog. Energy Combust. Sci.* **2013**, *39*, 61–110. [CrossRef]
32. Popov, N.A. Kinetics of plasma-assisted combustion: Effect of non-equilibrium excitation on the ignition and oxidation of combustible mixtures. *Plasma Sources Sci. Technol.* **2016**, *25*, 043002. [CrossRef]
33. Pietanza, L.D.; Colonna, G.; Capitelli, M. Activation of vibrational-induced CO_2 dissociation in cold non-equilibrium plasma. *Plasma Phys. Control. Fusion* **2023**, *65*, 044004. [CrossRef]
34. Kadochnikov, I.N.; Arsentiev, I.V.; Loukhovitski, B.I.; Sharipov, A.S. State-to-state vibrational kinetics of diatomic molecules in laser-induced ignition of a syngas-air mixture: Modeling study. *Chem. Phys.* **2022**, *562*, 111669. [CrossRef]
35. Mankelevich, Y.A.; Rakhimova, T.V.; Voloshin, D.G.; Chukalovskii, A.A. Vibrationally Excited Ozone in Kinetics of O/N/Ar Mixtures after Ozone Photolysis. *Russ. J. Phys. Chem. A* **2023**, *97*, 1033–1045. [CrossRef]
36. Capitelli, M.; Ferreira, C.M.; Gordiets, B.F.; Osipov, A.I. *Plasma Kinetics in Atmospheric Gases*; Springer Series on Atomic, Optical, and Plasma Physics; Springer: Berlin/Heidelberg, Germany, 2000; Volume 31.
37. Veselinova, A.; Agúndez, M.; Goicoechea, J.R.; Menéndez, M.; Zanchet, A.; Verdasco, E.; Jambrina, P.; Aoiz, F.J. Quantum study of reaction $O(^3P)+H_2(v,j)\rightarrow OH+H$: OH formation in strongly UV-irradiated gas. *Astron. Astrophys.* **2021**, *648*, A76. [CrossRef] [PubMed]
38. Zannese, M.; Tabone, B.; Habart, E.; Goicoechea, J.R.; Zanchet, A.; van Dishoeck, E.F.; van Hemert, M.C.; Black, J.H.; Tielens, A.G.; Veselinova, A.; et al. OH as a probe of the warm-water cycle in planet-forming disks. *Nat. Astron.* **2024**. [CrossRef]
39. Truhlar, D.G.; Muckerman, J.T. Reactive scattering cross sections III: Quasiclassical and semiclassical methods. In *Atom-Molecule Collision Theory: A Guide for the Experimentalist*; Springer: Berlin/Heidelberg, Germany, 1979; pp. 505–566.
40. Gray, S.K.; Balint-Kurti, G.G. Quantum dynamics with real wave packets, including application to three-dimensional (J = 0) D + H_2 = HD + H reactive scattering. *J. Chem. Phys.* **1998**, *108*, 950–962. [CrossRef]
41. Gorse, C.; Capitelli, M.; Bacal, M.; Bretagne, J.; Laganà, A. Progress in the non-equilibrium vibrational kinetics of hydrogen in magnetic multicusp H-ion sources. *Chem. Phys.* **1987**, *117*, 177–195. [CrossRef]
42. Pogosbekian, M.J.; Sergievskaia, A.L.; Losev, S.A. Verification of theoretical models of chemical exchange reactions on the basis of quasiclassical trajectory calculations. *Chem. Phys.* **2006**, *328*, 371–378. [CrossRef]
43. Esposito, F.; Armenise, I.; Capitelli, M. N–N_2 state to state vibrational-relaxation and dissociation rates based on quasiclassical calculations. *Chem. Phys.* **2006**, *331*, 1–8. [CrossRef]
44. Bender, J.D.; Valentini, P.; Nompelis, I.; Paukku, Y.; Varga, Z.; Truhlar, D.G.; Schwartzentruber, T.; Candler, G.V. An improved potential energy surface and multi-temperature quasiclassical trajectory calculations of N_2 + N_2 dissociation reactions. *J. Chem. Phys.* **2015**, *143*. [CrossRef] [PubMed]
45. Andrienko, D.A.; Boyd, I.D. State-specific dissociation in O_2–O_2 collisions by quasiclassical trajectory method. *Chem. Phys.* **2017**, *491*, 74–81. [CrossRef]
46. Macdonald, R.L.; Jaffe, R.L.; Schwenke, D.W.; Panesi, M. Construction of a coarse-grain quasi-classical trajectory method. I. Theory and application to N_2–N_2 system. *J. Chem. Phys.* **2018**, *148*. [CrossRef] [PubMed]
47. Vargas, J.; Monge-Palacios, M.; Lacoste, D.A. State-Specific Dissociation and Inelastic Rate Constants for Collisions of H_2 with H and He. *J. Thermophys. Heat Transf.* **2023**. [CrossRef]

48. Garrido, J.d.D.; Ballester, M.Y. A Theoretical Study of the N_2+H_2 Reactive Collisions for High Vibrational and Translational Energies. *Atmosphere* **2021**, *12*, 1349. [CrossRef]
49. Hong, Q.; Bartolomei, M.; Coletti, C.; Lombardi, A.; Sun, Q.; Pirani, F. Vibrational Energy Transfer in CO + N_2 Collisions: A Database for V–V and V–T/R Quantum-Classical Rate Coefficients. *Molecules* **2021**, *26*, 7152. [CrossRef]
50. Tu, Z.; Li, J.; Wang, Y.; Song, H. Quasi-Classical Trajectory Dynamics Study of the Reaction OH + H_2S→H_2O + SH and Its Isotopic Variants: Comparison with Experiment. *Symmetry* **2023**, *15*, 256. [CrossRef]
51. Espinosa-Garcia, J.; Rangel, C.; Garcia-Chamorro, M.; Corchado, J.C. Quasi-Classical Trajectory Study of the CN+NH_3 Reaction Based on a Global Potential Energy Surface. *Molecules* **2021**, *26*, 994. [CrossRef] [PubMed]
52. Celiberto, R.; Capitelli, M.; Colonna, G.; D'Ammando, G.; Esposito, F.; Janev, R.K.; Laporta, V.; Laricchiuta, A.; Pietanza, L.D.; Rutigliano, M.; et al. Elementary Processes and Kinetic Modeling for Hydrogen and Helium Plasmas. *Atoms* **2017**, *5*, 18. [CrossRef]
53. Kuntz, P.J.; Nemeth, E.M.; Polanyi, J.C.; Rosner, S.D.; Young, C.E. Energy distribution among products of exothermic reactions. II. Repulsive, mixed, and attractive energy release. *J. Chem. Phys.* **1966**, *44*, 1168–1184. [CrossRef]
54. Sharipov, A.S.; Loukhovitski, B.I. Energy disposal into the vibrational degrees of freedom of bimolecular reaction products: Key factors and simple model. *Chem. Phys.* **2021**, *544*, 111098. [CrossRef]
55. Dawes, R.; Thompson, D.L.; Guo, Y.; Wagner, A.F.; Minkoff, M. Interpolating moving least-squares methods for fitting potential energy surfaces: Computing high-density potential energy surface data from low-density ab initio data points. *J. Chem. Phys.* **2007**, *126*. [CrossRef]
56. Jiang, B.; Li, J.; Guo, H. Potential energy surfaces from high fidelity fitting of ab initio points: The permutation invariant polynomial-neural network approach. *Int. Rev. Phys. Chem.* **2016**, *35*, 479–506. [CrossRef]
57. Meuwly, M. Machine Learning for Chemical Reactions. *Chem. Rev.* **2021**, *121*, 10218–10239. [CrossRef] [PubMed]
58. Manzhos, S.; Carrington, T.J. Neural Network Potential Energy Surfaces for Small Molecules and Reactions. *Chem. Rev.* **2021**, *121*, 10187–10217. [CrossRef] [PubMed]
59. Braunstein, M.; Adler-Golden, S.; Maiti, B.; Schatz, G. Quantum and classical studies of the O(^3P)+H_2(v=0–3. j=0)→OH+H reaction using benchmark potential surfaces. *J. Chem. Phys.* **2004**, *120*, 4316–4323. [CrossRef]
60. Wang, W.; Rosa, C.; Brandão, J. Theoretical studies on the O(^3P)+H_2 →OH+H reaction. *Chem. Phys. Lett.* **2006**, *418*, 250–254. [CrossRef]
61. Xu, Z.H.; Zong, F.J.; Han, B.R.; Dong, S.H.; Liu, J.Q.; Ji, F. Effects of a reagent's rotational and vibrational excitations on reaction O(^3P)+H_2(ν = 0, 3, j = 0, 3, 5, 7, 9, 12, 15)→OH+H. *Chin. Phys. B* **2012**, *21*, 093103. [CrossRef]
62. Granovsky, A.A. Extended Multi-Configuration Quasi-Degenerate Perturbation Theory: The New Approach to Multi-state Multi-Reference Perturbation Theory. *J. Chem. Phys.* **2011**, *134*, 214113. [CrossRef]
63. Pelevkin, A.V.; Loukhovitski, B.I.; Sharipov, A.S. Reaction of H_2 with O_2 in excited electronic states: Reaction pathways and rate constants. *J. Phys. Chem. A* **2017**, *121*, 9599–9611. [CrossRef]
64. Pelevkin, A.V.; Sharipov, A.S. Reactions of electronically excited molecular nitrogen with H_2 and H_2O molecules: Theoretical study. *J. Phys. D Appl. Phys.* **2018**, *51*, 184003. [CrossRef]
65. Pelevkin, A.V.; Loukhovitski, B.I.; Sharipov, A.S. Interaction of Electronically Excited CO ($a^3\Pi_r$) Molecules with H, H_2, and H_2O: Potential Energy Surfaces and Reaction Kinetics. *Phys. Chem. Res.* **2023**, *11*, 837–851.
66. Sharipov, A.S.; Loukhovitski, B.I.; Pelevkin, A.V.; Korshunova, M.R. A detailed kinetic submechanism for OH* chemiluminescence in hydrogen combustion revisited. Part 1. *Combust. Flame* **2024**, *263*, 113407. [CrossRef]
67. Deskevich, M.P.; Nesbitt, D.J. Dynamically weighted multiconfiguration self-consistent field: Multistate calculations for F+H_2O→HF+OH reaction paths. *J. Chem. Phys.* **2004**, *120*, 7281. [CrossRef] [PubMed]
68. Pelevkin, A.V.; Loukhovitski, B.I.; Sharipov, A.S. Reaction of the N Atom with Electronically Excited O_2 Revisited: A Theoretical Study. *J. Phys. Chem. A* **2021**, *125*, 8294–8312. [CrossRef] [PubMed]
69. Kendall, R.A.; Dunning, T.H., Jr.; Harrison, R.J. Electron Affinities of the First-Row Atoms Revisited. Systematic Basis Sets and Wave Functions. *J. Chem. Phys.* **1992**, *96*, 6796–6806. [CrossRef]
70. Helgaker, T.; Klopper, W.; Koch, H.; Noga, J. Basis-set convergence of correlated calculations on water. *J. Chem. Phys.* **1997**, *106*, 9639–9646. [CrossRef]
71. Halkier, A.; Helgaker, T.; Jørgensen, P.; Klopper, W.; Olsen, J. Basis-set convergence of the energy in molecular Hartree–Fock calculations. *Chem. Phys. Lett.* **1999**, *302*, 437–446. [CrossRef]
72. Lesiuk, M.; Jeziorski, B. Complete basis set extrapolation of electronic correlation energies using the Riemann zeta function. *J. Chem. Theory Comput.* **2019**, *15*, 5398–5403. [CrossRef]
73. Granovsky, A.A. Firefly V. 8.2.0. 2016. Available online: http://classic.chem.msu.su/gran/firefly/index.html (accessed on 1 June 2024).
74. Schmidt, M.W.; Baldridge, K.K.; Boatz, J.A.; Elbert, S.T.; Gordon, M.S.; Jensen, J.H.; Koseki, S.; Matsunaga, N.; Nguyen, K.A.; Su, S.; et al. General Atomic and Molecular Electronic Structure System. *J. Comput. Chem.* **1993**, *14*, 1347–1363. [CrossRef]
75. Abadi, M.; Agarwal, A.; Barham, P.; Brevdo, E.; Chen, Z.; Citro, C.; Corrado, G.S.; Davis, A.; Dean, J.; Devin, M.; et al. TensorFlow: Large-Scale Machine Learning on Heterogeneous Systems, Software. 2015. Available online: https://www.tensorflow.org/ (accessed on 1 June 2024).

76. Paszke, A.; Gross, S.; Chintala, S.; Chanan, G.; Yang, E.; DeVito, Z.; Lin, Z.; Desmaison, A.; Antiga, L.; Lerer, A. Automatic differentiation in PyTorch. In Proceedings of the 31st Conference on Neural Information Processing Systems (NIPS 2017), Long Beach, CA, USA, 4–9 December 2017.
77. Chollet, François and Others. Keras. GitHub. 2015. Available online: https://github.com/fchollet/keras (accessed on 1 June 2024).
78. Braams, B.J.; Bowman, J.M. Permutationally invariant potential energy surfaces in high dimensionality. *Int. Rev. Phys. Chem.* **2009**, *28*, 577–606. [CrossRef]
79. Bosma, W.; Cannon, J.; Playoust, C. The Magma algebra system I: The user language. *J. Symb. Comput.* **1997**, *24*, 235–265. [CrossRef]
80. Decker, W.; Greuel, G.M.; Pfister, G.; Schönemann, H. Singular 4-1-2—A Computer Algebra System for Polynomial Computations. 2019. Available online: http://www.singular.uni-kl.de (accessed on 1 June 2024).
81. Polak, L.S.; Goldenberg, M.J.; Levickij, A.A. *Vychislitel'nye Metody v Himicheskoj Kinetike [Computational Methods in Chemical Kinetics]*; Nauka: Moscow, Russia, 1984.
82. Abdel-Halim, H.M.; Jaafreh, S.M. Reaction rate constants from classical trajectories of atom-diatomic molecule collisions. *Z. Naturforschung A* **2008**, *63*, 159–169. [CrossRef]
83. Le Roy, R.J. LEVEL: A computer program for solving the radial Schrödinger equation for bound and quasibound levels. *J. Quant. Spectrosc. Radiat. Transf.* **2017**, *186*, 167–178. [CrossRef]
84. Rogers, S.; Wang, D.; Kuppermann, A.; Walch, S. Chemically Accurate ab Initio Potential Energy Surfaces for the Lowest $^3A'$ and $^3A''$ Electronically Adiabatic States of O(^3P)+H_2. *J. Phys. Chem. A* **2000**, *104*, 2308–2325. [CrossRef]
85. Zanchet, A.; Menéndez, M.; Jambrina, P.G.; Aoiz, F.J. New global potential energy surfaces of the ground $^3A'$ and $^3A''$ states of the O(^3P)+H_2 system. *J. Chem. Phys.* **2019**, *151*. [CrossRef] [PubMed]
86. Varga, T.; Olm, C.; Nagy, T.; Zsély, I.G.; Valkó, É.; Pálvölgyi, R.; Curran, H.J.; Turányi, T. Development of a joint hydrogen and syngas combustion mechanism based on an optimization approach. *Int. J. Chem. Kinet.* **2016**, *48*, 407–422. [CrossRef] [PubMed]
87. Starik, A.M.; Sharipov, A.S.; Titova, N.S. Intensification of syngas ignition through the excitation of CO molecule vibrations: A numerical study. *J. Phys. D Appl. Phys.* **2010**, *43*, 245501. [CrossRef]
88. Atkinson, R.; Baulch, D.L.; Cox, R.A.; Hampson, J.R.F.; Kerr, J.A.; Troe, J. Evaluated Kinetic and Photochemical Data for Atmospheric Chemistry. Supplement IV. *J. Phys. Chem. Ref. Data* **1992**, *21*, 1125. [CrossRef]
89. Tsang, W.; Hampson, R.F. Chemical Kinetic Data Base for Combustion Chemistry. *J. Phys. Chem. Ref. Data.* **1986**, *15*, 1087–1280. [CrossRef]
90. Cohen, N.; Westberg, K.R. Chemical kinetic data sheets for high-temperature chemical reactions. *J. Phys. Chem. Ref. Data* **1983**, *12*, 531–590. [CrossRef]
91. Dove, J.E.; Teitelbaum, H. The vibrational relaxation of H_2. I. Experimental measurements of the rate of relaxation by H_2, He, Ne, Ar, and Kr. *Chem. Phys.* **1974**, *6*, 431–444. [CrossRef]
92. Cacciatore, M.; Capitelli, M.; Billing, G. Vibration-to-translation energy exchanges in H_2 colliding with highly vibrationally excited H_2 molecules. *Chem. Phys. Lett.* **1989**, *157*, 305–308. [CrossRef]
93. Millikan, R.C.; White, D.R. Systematics of vibrational relaxation. *J. Chem. Phys.* **1963**, *39*, 3209–3213. [CrossRef]

Disclaimer/Publisher's Note: The statements, opinions and data contained in all publications are solely those of the individual author(s) and contributor(s) and not of MDPI and/or the editor(s). MDPI and/or the editor(s) disclaim responsibility for any injury to people or property resulting from any ideas, methods, instructions or products referred to in the content.